Supporting information for

HCl-assisted fabrication of metal-organic framework UiO-66(Zr) for affordable gas capture

Zineb OUZROUR,[a] El mehdi MOUMEN,[b] Ran Eitan ABUTBUL,[c] Daniel LEE,[c] Marta FALKOWSKA,[c] Tausif ALTAMASH,[a] Samir EL HANKARI [b] and Johan JACQUEMIN [a,*]

a Materials Science and Nano-engineering (MSN) Department. Mohammed VI Polytechnic University (UM6P), Lot 660 - Hay Moulay Rachid, 43150, Benguerir, Morocco.

b Chemical and Biochemical Sciences (CBS) Department. Mohammed VI Polytechnic University (UM6P), Lot 660 - Hay Moulay Rachid, 43150, Benguerir, Morocco.

c Department of Chemical Engineering, University of Manchester (UoM), Oxford Rd, Manchester M13 9PL, United Kingdom.

Corresponding author email: Johan.jacquemin@um6p.ma

.

Experimental Section

Materials:

Zirconium tetrachloride ($ZrCl_4$, > 99.95%), Zirconyl oxychloride hexahydrate ($ZrOCl_2.8H_2O$) N,N-dimethylformamide (DMF, A.R. grade), ethanol (C_2H_5OH, A.R. grade), terephthalic acid (H_2BDC, 98%), were obtained from Sigma Aldrich Chemicals and were used without further purification. CO_2 (> 99.997%) was provided by Air Liquide Morocco.

Compound	**Purity**	**Quantity**	**Price (€)**	**Price per kg (€)**	**Source**	Ref
$ZrOCl_2{\cdot}8H_2O$	98%	500 g	654	1,308	Sigma-Aldrich	224316
$ZrCl_4$	≥99.9% (trace metals basis)	100 g	350	3,500	Sigma-Aldrich	357405

Synthesis of 2-UiO-66

In a 120 mL vial, 483 mg of $ZrOCl_2{\cdot}8H_2O$, 10 mL of DMF were loaded; the resulting mixture was sonicated for 20 min to ensure that all reactants were completely dissolved and mixed. In a separate 120 mL vial, 249 mg of terephthalic acid and 20 mL of DMF were loaded and sonicated for 10 min. The contents of this vial were then poured into the above mixture, followed by an additional sonication for 20 min. This was followed by heating at 120 °C for 24 h to ensure an effective formation of UiO-66 particles. The resulting product was filtered off, washed first with DMF (4 × 30 mL) and then with EtOH (3 × 30 mL) to remove the excess of unreacted organic linkers. The final product was dried in a vacuum oven at 60 °C for 24 h before being analyzed.

Synthesis of 1-UiO-66

In a 120 mL vial, 349.5 mg of $ZrCl_4$, 10 mL of DMF and 1 mL of HCl were loaded; the resulting mixture was sonicated for 20 min. In a separate 120mL vial, 249 mg of terephthalic acid and 20 mL of DMF were loaded and sonicated for 10 min. The contents of this vial were then added into the above mixture, and sonicated for 20 min. This was followed by heating at 120 °C for 24 h. The resulting product was filtered off, washed first with DMF (4 × 30 mL) and then with EtOH (3 × 30 mL) to remove the excess of unreacted organic linkers. The final product was dried in a vacuum oven at 60 °C for 24 h before being analyzed.

Synthesis of 2-UiO-66-HCl

In a 120 mL vial, 483 mg of $ZrOCl_2 \cdot 8H_2O$, 10 mL of DMF and 1 mL of HCl were loaded; the resulting mixture was sonicated for 20 min. In a separate 120 mL vial, 249 mg of terephthalic acid and 20 mL of DMF were loaded and sonicated for 10 min. The contents of this vial were then added into the above mixture, and sonicated for 20 min. This was followed by heating at 120 °C for 24 h. The resulting product was filtered off, washed first with DMF (4 × 30 mL) and then with EtOH (3 × 30 mL) to remove the excess of unreacted organic linkers. The final product was dried in a vacuum oven at 60 °C for 24 h before being analyzed.

Visual aspects of the 3 powders

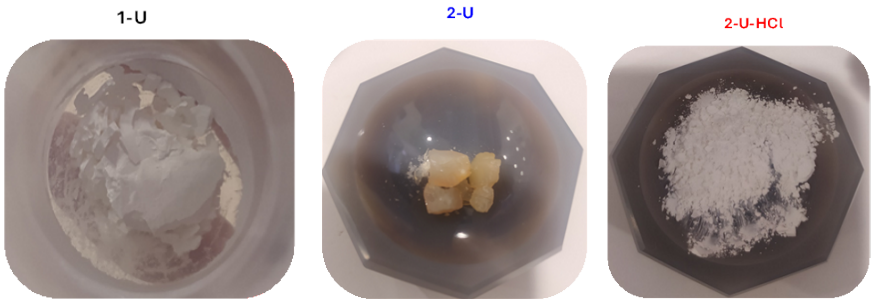

Characterization Methods

-The crystallinity of the samples was evaluated using a Bruker-AXS D8 powder diffractometer with a Cu Kα radiation (λKα = 0.154186 nm). The studied samples were ground to a fine powder, prepared carefully in an XRD sample holder to create a flat upper surface, and then operated in the range of 5° and 80° (2 Theta) with a sample holder rotation of 30 rpm to avoid the preferential orientations.

-The morphologies and structure of tested samples were examined using a scanning electron microscope (SEM, JSM-7200F/LV) operated at 1 and 5 kV.

-The thermal stability and the degradation behavior of all samples were evaluated by thermogravimetric analysis (TGA) using TGA instruments equipment (Discovery TGA). Samples were heated from room temperature to 700°C at a heating rate of 5 °C·min^{-1}. All measurements were performed in air with a flow of 10 mL·min^{-1} to allow oxidation effects.

CO_2 adsorption measurements

Adsorption isotherms of pure CO_2 in tested samples were obtained using a SETARAM Gaspro GA equipment set at a constant temperature (i.e. T = 20 or 25 °C ± 1 °C) at variant pressure 0-1 bar (see Fig. S1). Typically, approx. 0.05-0.1 g of sorbent was fed into this equilibrium cell, while the

exact mass of each tested sample was determined before and after each set of measurements to avoid any error associated with weight loss after its activation. However, before running any solubility measurement, the volume of the equilibrium cell containing the activated sample, set at a constant temperature (20 or 25°C), was determined thanks to a volume calibration using Helium gas prior to being degassed again. Then, a series of two pVT measurements were realized to know: i) the exact amount of CO_2 in gas phase put into contact of the activated material prior to the adsorption and ii) after reaching the thermodynamic equilibrium for each tested real gas thermodynamic condition. The quantity of CO_2 adsorbed (or desorbed) by the material is thus simply obtained by a simple subtraction of these two pVT measurements by considering also any potential temperature change within such measurements. As all tests realized therein were run under an isothermal mode into an isochoric equipment, the progress of any measurement was thus monitored thanks to the variation of the pressure (bar) over the time (s) until reaching the equilibrium (i.e. p = constant). In the case of the adsorption measurements, when an equilibrium was reached, the pressure was thus increased by adding into the equilibrium cell a well-known quantity of pure CO_2 (DP = 0.1 bar) until reaching an absolute total pressure of 1 bar. In the case of the desorption measurements, simple expansion measurements were done by reaching a novel thermodynamic equilibrium by decreasing the total gas pressure in the whole equipment. The activation of the three samples (1-U, 2-U, 2-U-HCl) was done at 120 °C under vacuum (i.e. at pressure of 1 Pa). While in the case of the 2-U-HCl sample, when the activation temperature was set at 300 °C for 4 h or 12 h, each tested sample was first activated in a muffle furnace followed by an activation in the isochoric instrument by following the same conditions as above-mentioned.

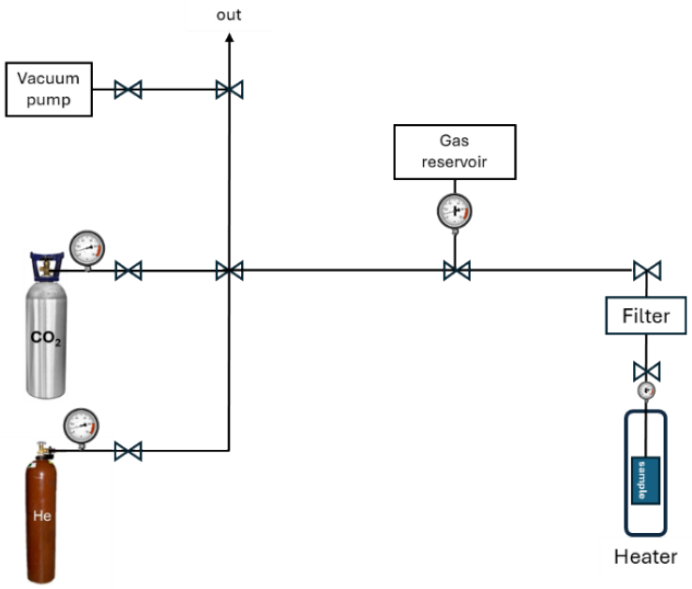

Schema 1. SETERAM isochoric equipment used for the determination of the CO_2 adsorption in tested UiO-66 samples.

Isotherms of adsorption

- **Langmuir Isotherm**

The Langmuir model is based on the assumption that adsorption occurs on a homogeneous surface with a finite number of identical sites, and once a site is occupied, no further adsorption occurs. It also assumes there is no interaction between adsorbed molecules and that adsorption follows a dynamic equilibrium between adsorbed and desorbed molecules[1].

$$q_e = \frac{(q_{max}.K_L.P_e)}{(1 + K_L.P_e)} \quad (1)$$

q_e = amount of gas adsorbed per unit mass of adsorbent (mmol·g^{-1})

q_{max} = maximum adsorption capacity (mmol·g^{-1})

K_L = Langmuir equilibrium constant (bar^{-1})

P_e = equilibrium pressure of the adsorbate (bar)

- **Freundlich Isotherm**

The Freundlich model is an empirical equation that assumes adsorption occurs on a heterogeneous surface with varying adsorption sites and multilayer adsorption. The adsorption energy decreases logarithmically as coverage increases[1].

$$q_e = K_F\, Pe^{(1/n)} \quad (2)$$

q_e = amount of gas adsorbed per unit mass of adsorbent (mmol/g)($bar^{-1/n}$)

K_F = Freundlich equilibrium constant (bar^{-1})

P_e = equilibrium pressure of the adsorbate (bar)

n = adsorption intensity constant (dimensionless)

Error calculation

Each error bar was determined using an error propagation method including instrumental, experimental and weighing relative uncertainties.

For the Setaram GASPRO-HA equipped with a Microdoser and a K-type thermocouple at 298 K, the PVT relative uncertainties are as follows:

- pressure transducer (0-15 bar head): 0.12% of reading,
- K-type thermocouple: $\pm$ 1 K (i.e. 0.34% at 293-298 K),
- calibrated reservoir and system volumes: 1% and 3.32% respectively,

while the compressibility factor uncertainty was neglected as the equilibrium pressure is always close to atmospheric.

By considering Demirocak et al.[2] and by using these error values, the instrumental relative uncertainty was found to be $u_{r,\ machine}$ = 0.035.

In the case of the experimental uncertainty, the data collected for the 2-U-HCl sample were used, herein as a reference, to assess the standard deviation associated to the measurement repeatability. This sample was chosen because its repeatability could be directly assessed in a statistical sense, and it showed the largest overall uncertainty. Furthermore, by using this equipment, it is practically impossible to reach common fixed equilibrium pressure points when replicating gas solubility measurements. For that reason, each dataset was first correlated to recalculate CO_2 uptake values to common pressures. Then, at each pressure, the experimental relative uncertainty, $u_{r,exp.}$, was then calculated using the raw data reported in Table S6 along with the equations 3 to 5.

$$q = \frac{1}{n}\sum_{r=1}^{n} qr \tag{3}$$

where; q (mmol·g^{-1}) is the average CO_2 uptake across all n independent replicates qr (mmol/g) values at a set pressure.

$$s_d = \sqrt{\frac{1}{n-1}\sum_{r=1}^{n}(qr - q)^2} \quad (4)$$

where s_d (mmol·g^{-1}) is the standard deviation of the CO_2 uptake.

$$u_{r,exp.} = \frac{s_d}{q} \quad (5)$$

For example, in the case of data reported in row 2 of the Table S7, i.e. s_d = 0.001 mmol·g^{-1} and q = 0.128 mmol·g^{-1}, $u_{r,exp.}$ = 0.008.

To ensure a fair and cautious analysis, equation 5 was used for each CO_2 uptake determined for all tested materials by keeping constant the s_d values as determined with the reference 2-U-HCl sample.

The weighing relative uncertainty, $u_{r,m}$, was determined as follows,

$$u_{r,m} = \frac{s_m}{m} \quad (6)$$

where s_m is the standard deviation of the balance ($s_m =$ 1 mg) and m is the sample mass. For a sample of 49 mg, the weighing uncertainty corresponds to u_m= 1/49 = 0.02. Each $u_{r,m}$ value was propagated into total uncertainty together with uncertainties associated to both the machine and experimental measurements.

Finally, the total relative uncertainty, $u_{r,total}$, in CO_2 uptake was calculated as follows:

$$u_{r,total} = \sqrt{u_{r,exp.}^2 + u_{r,m}^2 + u_{r,machine}^2} \quad (7)$$

For example, by applying the example values (row 2 of the Table S7) in equation 7, the total relative uncertainty $u_{r,total}$ becomes:

$$u_{r,total} = \frac{u_{total}}{q} = \sqrt{\left(\frac{0.001}{0.128}\right)^2 + 0.02^2 + 0.035^2} = 0.041 \quad (8)$$

Thus,

$$u_{total} = u_{r,total} \times q = 0.041 \times 0.128 = 0.0052 \text{ mmol·g}^{-1} \quad (9)$$

This ensures that the total uncertainty reflects the cumulative influence of instrument precision, weighing error and replicate variability at the actual CO_2 uptake and pressure of each measurement.

Solid-State NMR

Solid-state NMR spectra were recorded using a Bruker 9.4 T (400 MHz ^{1}H Larmor frequency) AVANCE III spectrometer equipped with a 4 mm HFX MAS probe. Experiments were acquired at ambient temperature using 12 kHz MAS frequencies. Samples were packed into 4 mm zirconia rotors under ambient conditions and sealed with a Kel-F rotor cap. The ^{1}H (π/2)- and π-pulse durations were 2.5 and 5.0 μs, respectively. The ^{13}C (π/2)- and π-pulse durations were 5.0 and 10.0 μs, respectively.

^{1}H MAS NMR spectra were recorded using an echo sequence, π/2-τ-π-τ, where the echo time (τ) was set to one rotor period, using a repetition delay of 1 s for 16 co-added transients. ^{13}C MAS NMR spectra were recorded using {^{1}H-}^{13}C cross-polarization (CP) with an echo (τ-π-τ) of the total duration of two rotor periods. ^{13}C spin-locking was applied for 2 ms at ~50 kHz, with corresponding ramped (70 - 100%) ^{1}H spin-locking at ~70 kHz for CPMAS experiments. 100 kHz SPINAL-64 heteronuclear ^{1}H decoupling was used throughout signal acquisition.[3] 2304 transients were co-added for all samples, with repetition delays of 2.25 s.

^{1}H T_1 relaxation times of the investigated UiO-66 samples are reported in Table S1.

Table S1. ^{1}H T_1 relaxation times of the investigated UiO-66 samples, pre- and post-activation (170 °C overnight under dynamic vacuum).

Sample name	Pre [ms]	Post [ms]
1-U	250	NA
2-U	672	436
2-U-HCl	407	413

Results and Discussion

(a) (b)

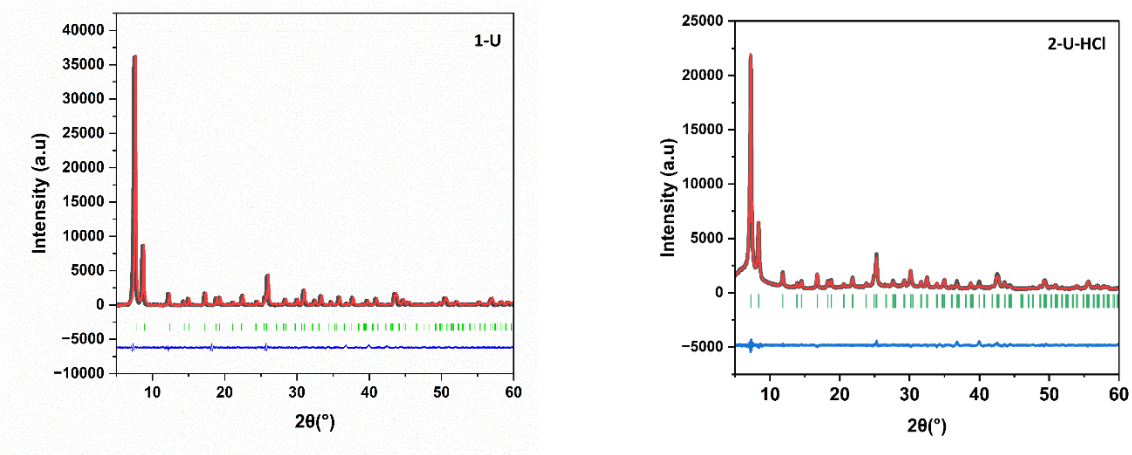

1.XRD fitting

Fig. S1. Powder XRD fits for a)1-U as-prepared and b) 2-U-HCl.

1. Defects calculation

To calculate the defects in each tested MOF framework some assumptions have been made. The remaining wt.% residue at 600 °C observed thanks to the TGA analysis was assumed to be composed uniquely of Zirconium (IV) oxide (ZrO_2). Therefore, it was assumed that at this temperature, all solvent, modulator and organic linker molecules were completely decomposed during the TGA analysis. Furthermore, it was assumed that the reaction scheme of the ideal UiO-66 decomposition is following reaction R1 as follows:

$$Zr_6O_6\,(BDC)_6\,(s) + 45\,O_2\,(g) \rightarrow 6\,ZrO_2\,(s) + 48\,CO_2\,(g) + 12\,H_2O\,(g) \qquad (R1)$$

During all calculations, a molar mass of the $Zr_6O_6(BDC)_6$ close to 1628.03 g·mol^{-1} was used, while that of six moles of ZrO_2 (123.22 g·mol^{-1}, each) was set to be close to 739.34 g·mol^{-1}.

Under these assumptions, the residual mass observed for each TGA trace at 600 °C was re-normalized to 100 % (i.e. using a factor of normalization = 100/wt% of remining mass at 600 °C) with respect to the methodology reported in the literature.[4]

Afterwards, it was then possible to calculate the number of defects (denoted x) by applying the following equations (10-12):

$$w_{Theo\ (Zr6O6\ (BDC)6)} = (1628.03 + 739.34) \times 100 = 220\ \% \qquad (10)$$

$$\frac{W_{exp(350\,°C)} - W_{exp(600\,°C)}}{220 - W_{exp(600\,°C)}} = \frac{6 - x}{6} \qquad (11)$$

$$x = 6 - \left(\left(\frac{W_{\exp\,(350\,^{\circ}C)} - W_{\exp\,(600\,^{\circ}C)}}{220 - W_{\exp\,(600\,^{\circ}C)}}\right) \times 6\right) \qquad (12)$$

(a) **(b)**

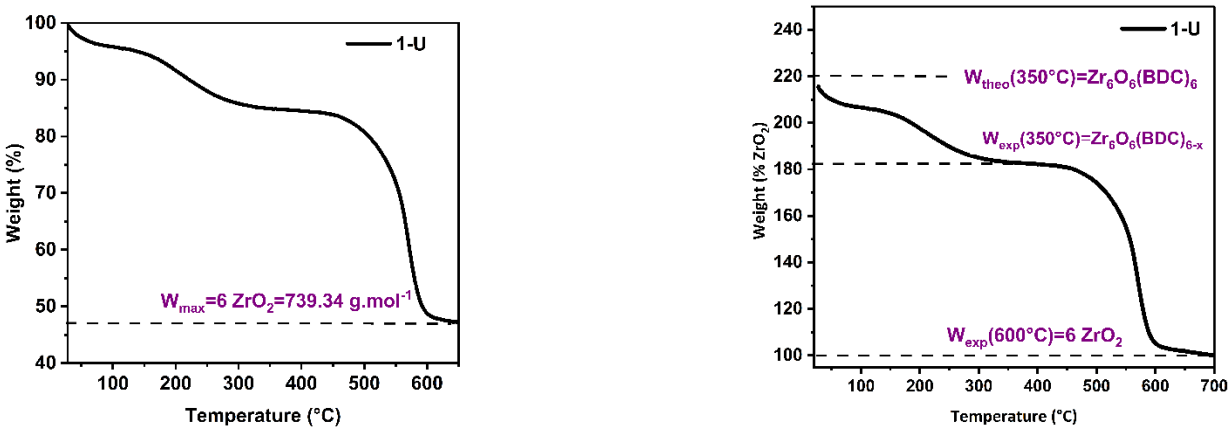

Fig. S2. a) TGA graph for 1-U as received, b) 1-U normalized TGA trace used to determine defects in UiO-66.

3.SEM images

a) b)

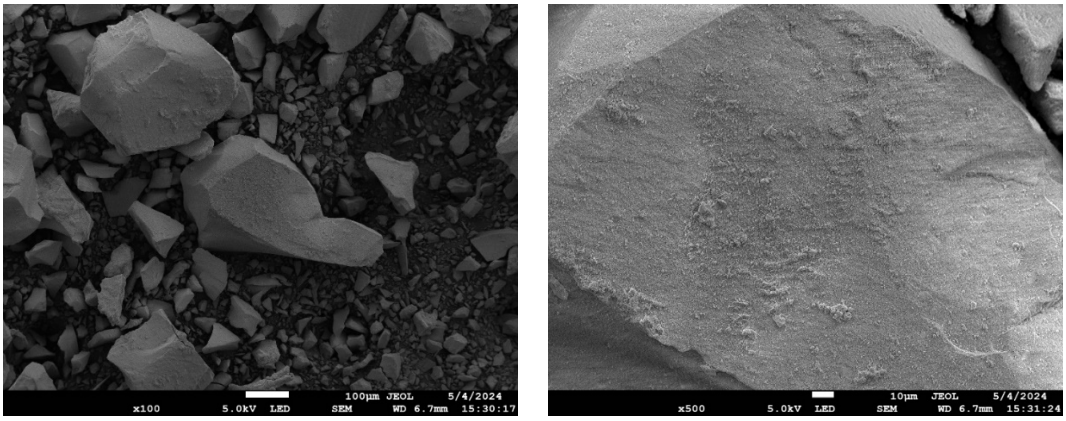

Fig. S3. SEM images of the 1-U sample within a scale bar of: a) 100 µm, b) 10 µm.

a) b)

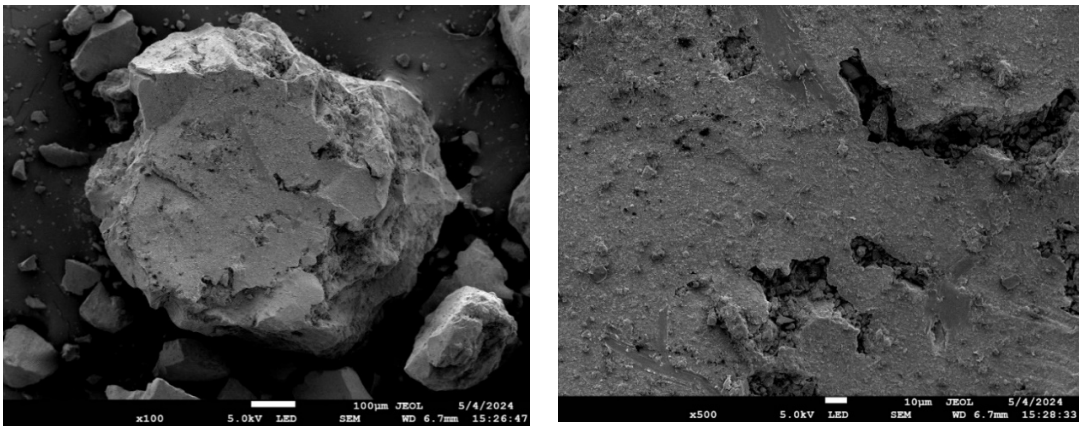

Fig. S4. SEM images of 2-U sample within a scale bar of: a) 100 µm, b) 10 µm.

a) b)

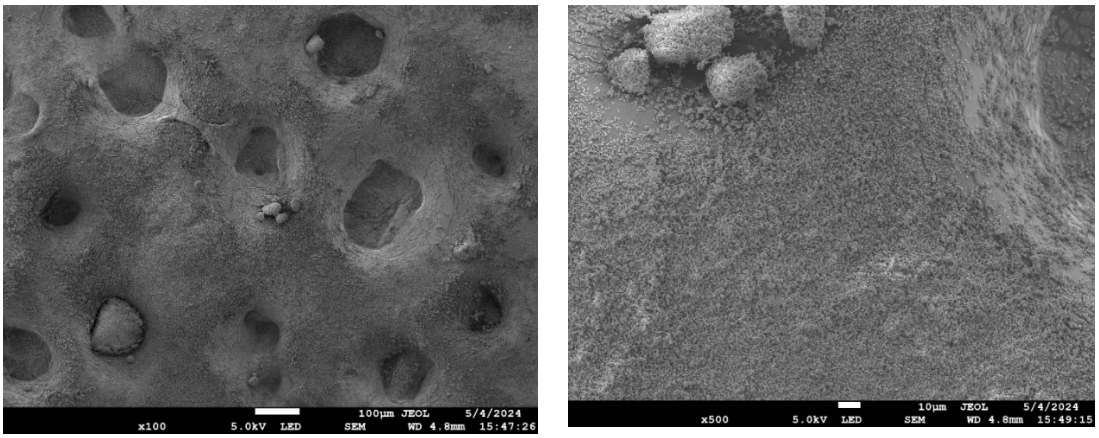

Fig. S5. SEM images of 2-U-HCl sample within a scale bar of: a) 100 µm, b) 10 µm.

4. N_2 adsorption desorption isotherm for tested samples

The N_2 adsorption measurements at 77 K were conducted on Micromeritics adsorption analyzer ASAP2060.

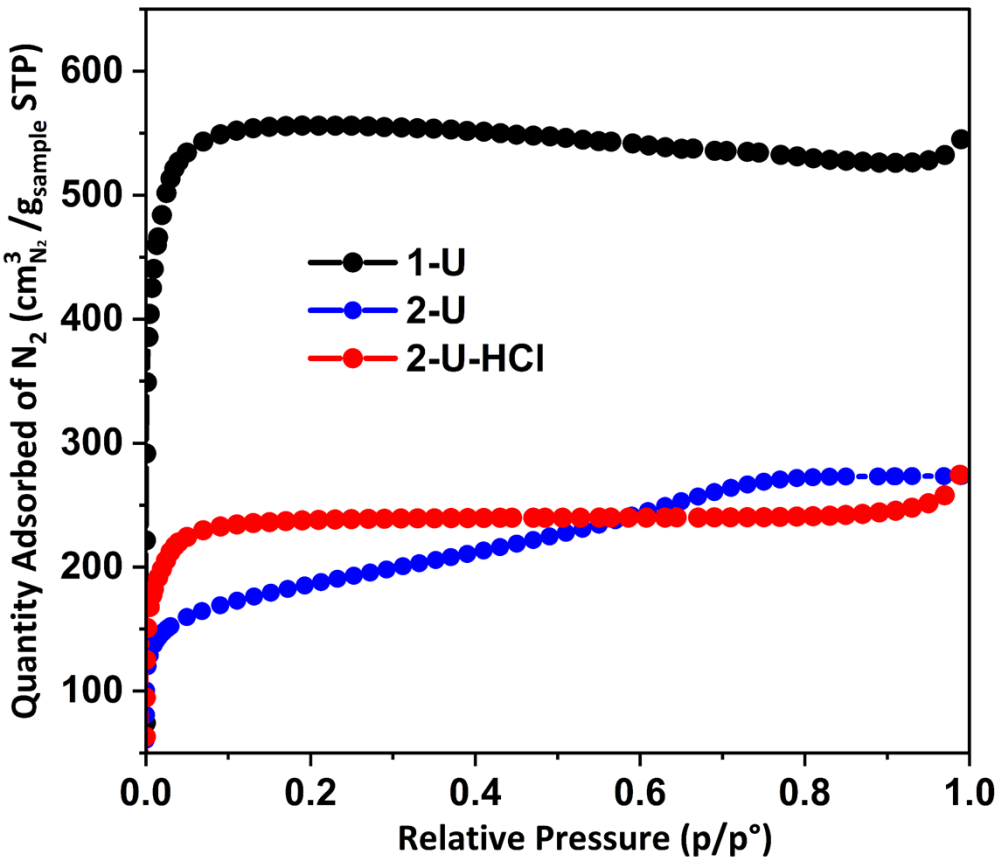

Fig. S6. N_2 adsorption-desorption isotherm measured at 77 K for 1-U: black ; 2-U: blue; 2-U-HCl: red. samples activated at 120°C for 12 h.

The N_2 adsorption measurements at 77 K were conducted on Micromeritics adsorption analyzer ASAP2060. As indicated in Table S2, different activation conditions were used prior to degassing under a dynamic vacuum at 0.1 bar using the Micromeritics adsorption analyzer ASAP2020.

Table S2. Surface area analysis of tested samples at different temperatures and degassing conditions.

Name of samples	Degassing temp, °C	Degassing time,	BET surface area,

		h	$m^2 \cdot g^{-1}$
1-U	120	4	683
2-U	120	4	561
	170	4	639
	170*	12 + 4	657
	300	4	646
2-U-HCl	120	4	583
	170	4	480
	170*	12 + 4	729
	300	4	654
	300*	12 + 4	805

Samples for measurements highlighted by * were activated in a two-stage process: (i) drying in a muffle furnace for 12 h in air, and (ii) degassing in adsorption analyzer for 4 h under vacuum (0.1 bar)

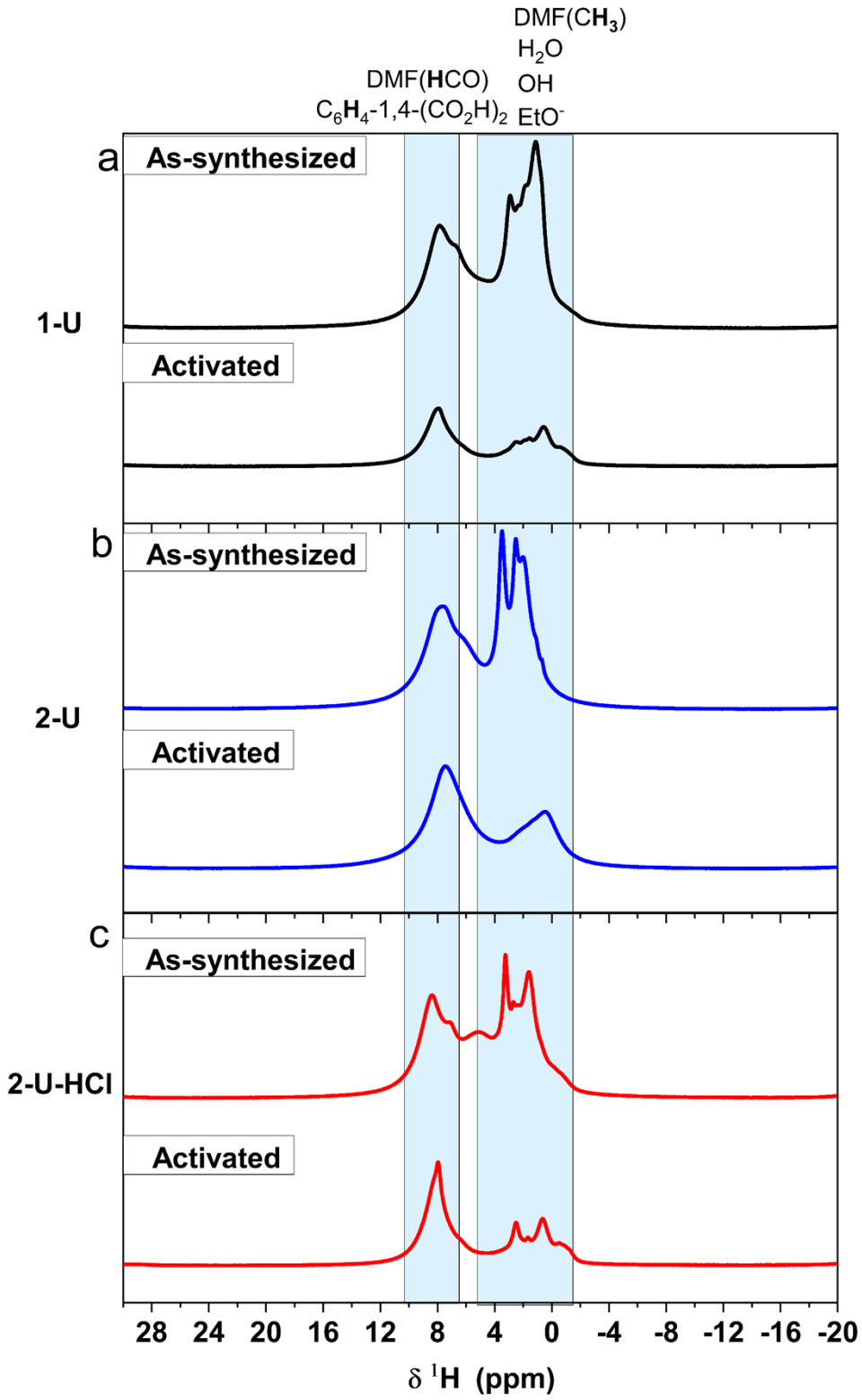

Fig. S7. ^{1}H MAS NMR spectra of the as-synthesized and activated (at 170°C for 12 h) materials: a)1-U; b) 2-U; c) 2-U-HCl.

5. XRD analysis

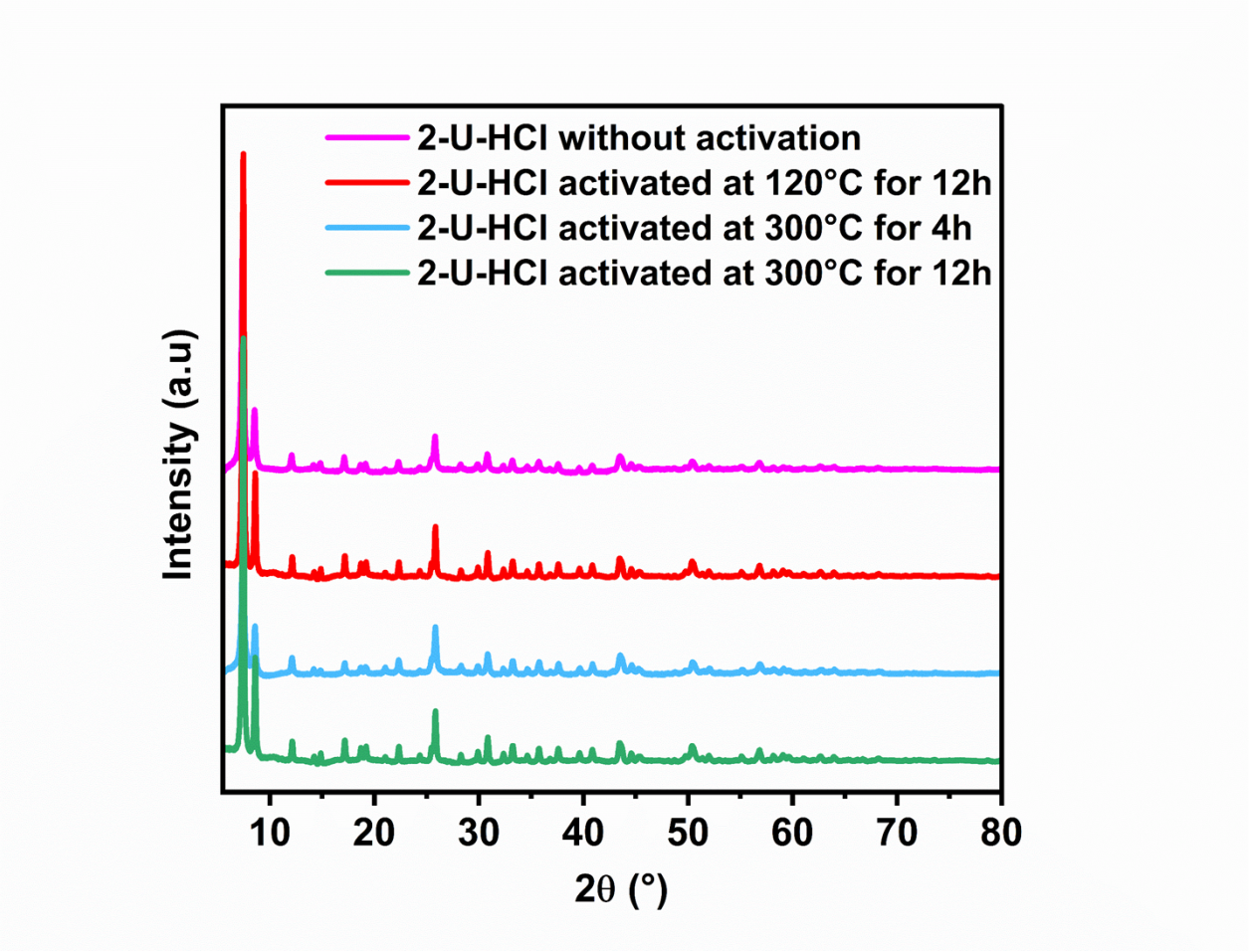

Fig. S8. Impact of the applied activation conditions on the XRD pattern of 2-U-HCl sample.

6. CO_2 absorption kinetic of tested samples at 20 °C and 1 bar

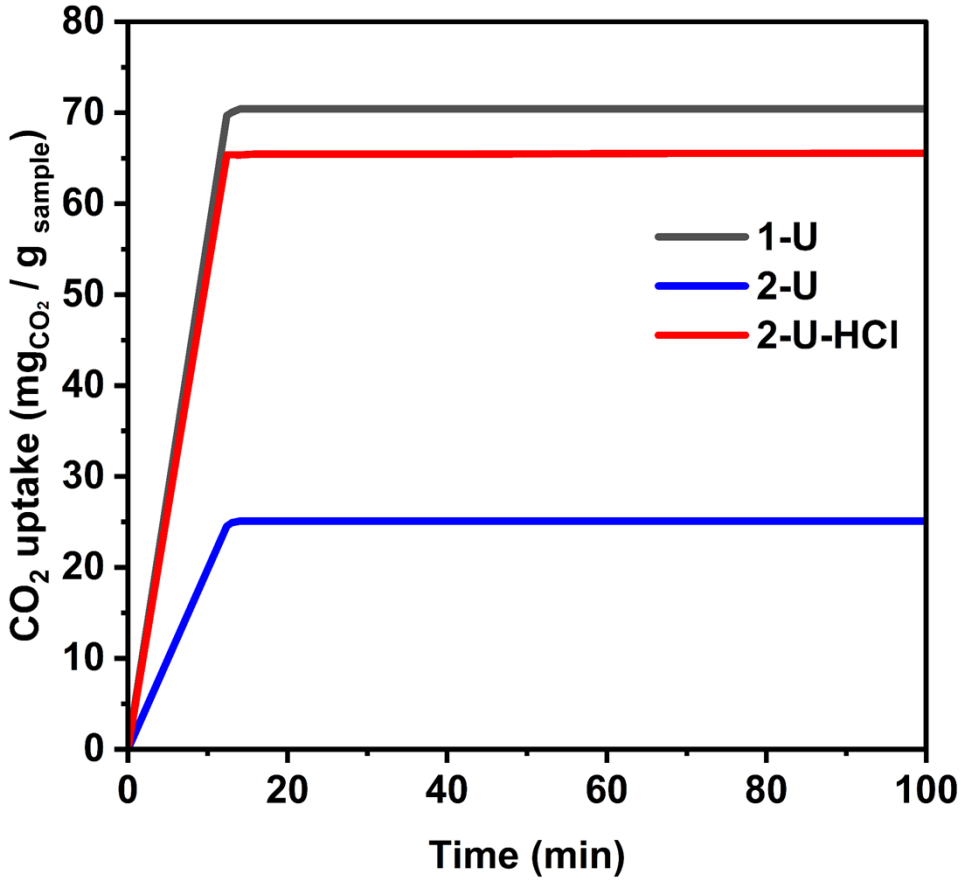

Fig. S9. CO_2 adsorption kinetics at 1 bar and 293 K for 1-U: black ; 2-U: blue; 2-U-HCl:red.

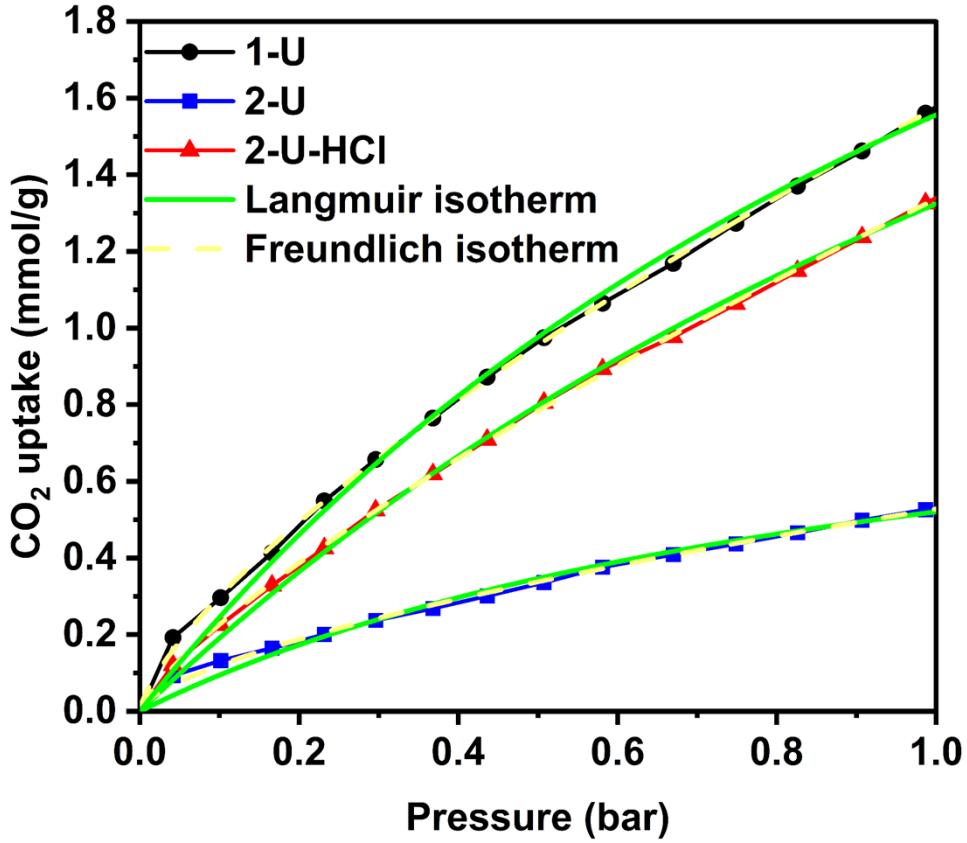

Fig. S10. CO_2 adsorption isotherms at 293 K and 1 bar for UiO-66 samples 1-U: black ; 2-U: blue; 2-U-HCl: red. Experimental data are plotted alongside Freundlich model: yellow dots and Langmuir model: green line.

Table S3. Fitting parameters for CO_2 adsorption isotherms of the UiO-66 samples 1-U, 2-U, and 2-U-HCl at 293 K.

	Freundlich Isotherm			Langmuir Isotherm		
	n	K_F (bar^{-1})	R^2	q_m ($mmol \cdot g^{-1}$)	K_L (bar^{-1})	R^2
1-U	1.33	1.17	99.98	2.65	0.76	99.32
2-U	1.47	0.39	99.03	0.91	0.74	98.08
2-U-HCl	1.44	1.42	99.85	3.91	0.56	99.64

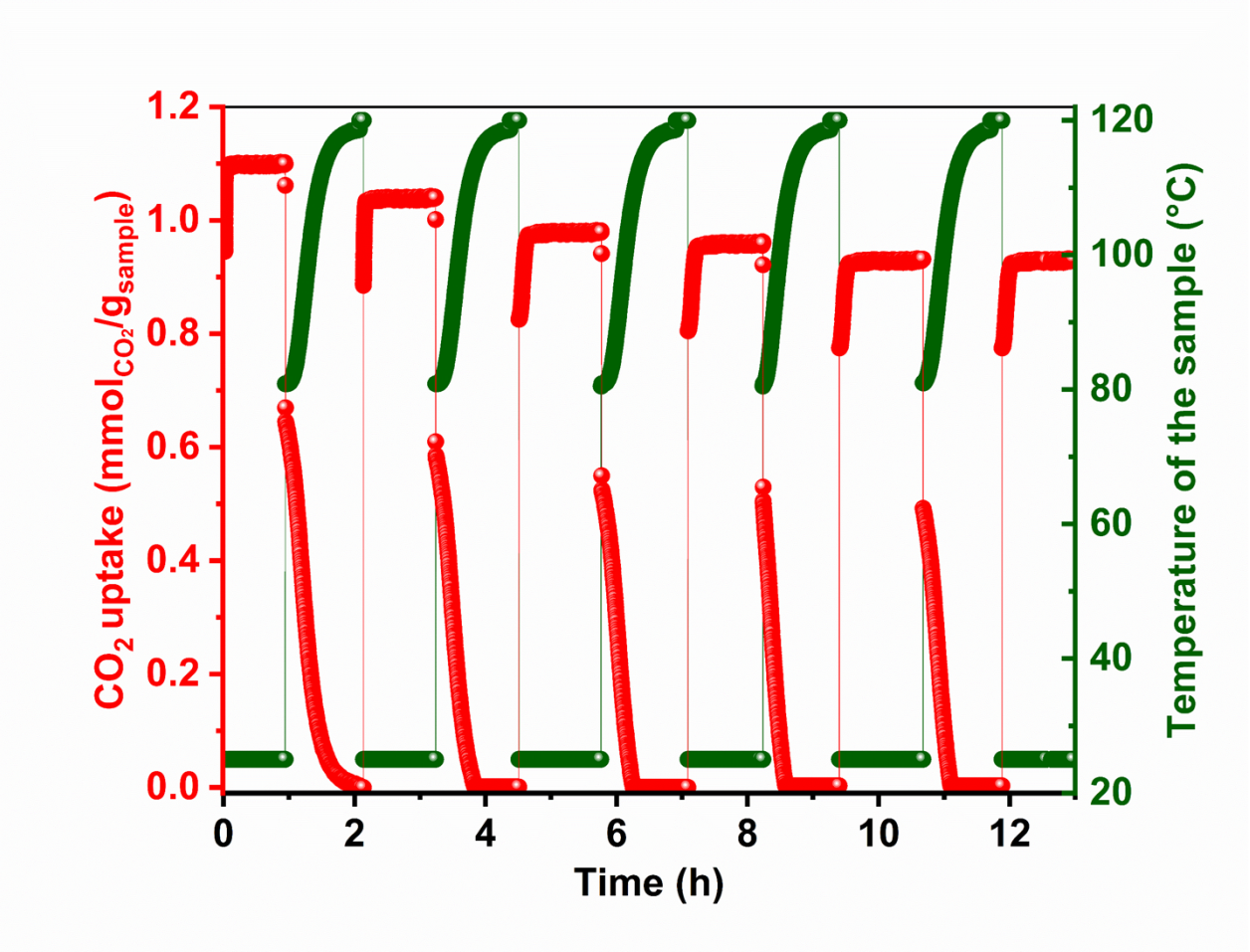

Fig. S11. CO_2 adsorption-desorption cycling performance of 2-U-HCl sample (red) over five consecutive cycles.

7. Impact of the activation temperature on 2-U-HCl sample the CO_2 adsorption capacity

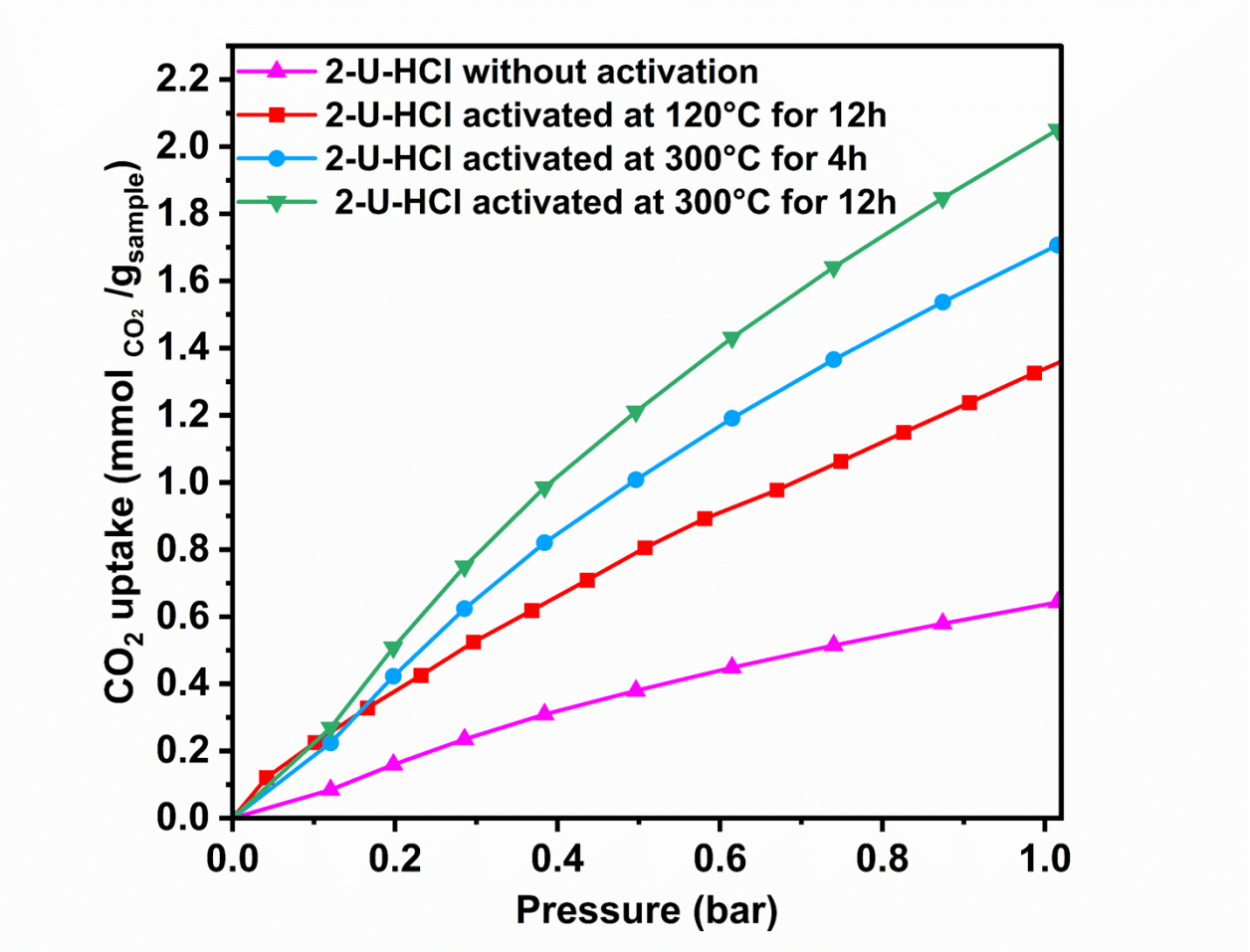

Fig. S12. Impact of the activation conditions applied on the CO_2 adsorption of the 2-U-HCl sample: purple, non-activated sample; red, activated at 120 °C during 12 h; light blue, activated at 300 °C during 4 h; green, activated at 300 °C during 12 h.

8. Comparison of the CO_2 adsorption capacity determined during this work and available in the literature

Table S4. Comparison of CO_2 adsorption data collected during this work for tested samples with those reported in the literature at 1 bar for UiO-66.

Name	Set temperature at the equilibrium (K)	Sample activation conditions		CO_2 uptake ($mmol \cdot g^{-1}$)	Reference
		Time (h)	Temperature (K)		
1-U	298	8	393	1.4	This work
2-U	298	8	393	0.4	This work
2-U-HCl	298	8	393	1.2	This work
2-U-HCl	293	12	673	2.1	This work
UiO-66	298	4	423	1.6	[5]
UiO-66	298	6	423	1.7	[6]
UiO-66	298	12	298	2.1	[7]
UiO-66	298	12	383	2.1	[8]
UiO-66	298	NA	NA	1.6	[9]

NA: Not available

Table S5. Comparison of CO_2 adsorption data with known MOF based on the literature.

MOF	S_{BET} ($m^2 \cdot g^{-1}$)	Equipment	CO_2 adsorption capacity ($mmol \cdot g^{-1}$)	Temperature (K)	Pressure (bar)	Reference
1-U	683	Setaram Gaspro SA	1.4	298	1	This work
2-U	561	Setaram Gaspro SA	0.4	298	1	This work
2-U-HCl	>729	Setaram Gaspro SA	2.1	293	1	This work
PAA@UiO-66	445	Micromeritics ASAP 2020 PLUS HD88	0.74	298	1	[10]
ZIF-8	1429.32	BELSORP-mini, MicrotracBEL	0.79	298	1	[11]
Cu-MOF	NA	NA	1.5	298	1	[12]
MOF-177	3977	Gravimetric set up	0.86	298	1	[13]
PCN-777	2008	BELSORP-max, Bel-Japan	1.13	298	1	[14]
M808	1742	BELSORP-max, Bel-Japan	1.38	298	1	[15]
UiO-67	2407.42	Micromeritics ASAP 2020	1.65	273	1	[16]
ZIF-8	1318	IsoSORP STATIC 3xV-MP	0.75	303	1	[17]
Mg-MOF-74	-	Micromeritics ASAP 2020	1.49	273	1	[18]
UiO-67	2407	Micromeritics ASAP 2020	1.06	273	1	[19]
ZIF-8	498	Setaram Gaspro SA	0.25	303	1	[20]
ZIF-67	280	Setaram Gaspro SA	0.61	303	1	[20]

NA: Not available

Table S6. Raw Data of CO_2 measurements

2-U-HCl (m=0.067 g)		2-U-HCl (m=0.049 g)	
CO_2 capacity (mol)	Eq. Pressure (bar)	CO_2 capacity (mol)	Eq. Pressure (bar)
0	0.016092	0	0.030805
$1.67.10^{-5}$	0.105262	$6.31.10^{-6}$	0.108317
$2.43.10^{-5}$	0.161636	$1.31.10^{-5}$	0.177363
$3.15.10^{-5}$	0.289318	$1.94.10^{-5}$	0.262752
$3.81.10^{-5}$	0.372488	$2.40.10^{-5}$	0.372795
$4.43.10^{-5}$	0.460018	$2.91.10^{-5}$	0.470268
$4.98.10^{-5}$	0.552584	$3.40.10^{-5}$	0.567305
$5.51.10^{-5}$	0.643093	$3.95.10^{-5}$	0.667687
$6.02.10^{-5}$	0.735898	$4.45.10^{-5}$	0.767072
$6.56.10^{-5}$	0.828882	$4.98.10^{-5}$	0.866439
$7.09.10^{-5}$	0.927199	$5.50.10^{-5}$	0.967581
$7.62.10^{-5}$	1.024262	$6.01.10^{-5}$	1.065019

Relative uncertainties of the equipment : $u_{r,T}$ = 0.34 %, $u_{res,v}$ = 1 % , $u_{sys,v}$ = 3.32 %; $u_{r,p}$= 0.12 % for 0-15 bar

Table S7. Uncertainty values listed using the error propagation method to determine CO_2 uptake error bars reported in Figure 6.

P_{eq}	q	s_d	U_r	$U_{machine}$	U_m
0	0.000	0.000	NA	0.035	0.02
0.0308	0.128	0.001	0.01	0.035	0.02
0.108	0.258	0.013	0.05	0.035	0.02
0.177	0.379	0.023	0.06	0.035	0.02
0.262	0.529	0.056	0.11	0.035	0.02
0.372	0.628	0.048	0.08	0.035	0.02
0.470	0.719	0.035	0.05	0.035	0.02
0.567	0.814	0.012	0.01	0.035	0.02
0.667	0.903	0.007	0.01	0.035	0.02
0.767	0.998	0.026	0.03	0.035	0.02
0.866	1.090	0.045	0.04	0.035	0.02
0.967	1.182	0.063	0.05	0.035	0.02
1.065	1.220	0.009	0.01	0.035	0.02

References

1 A. Nayak, S. Viegas, H. Dasari and N. Sundarabal, *ACS Omega*, 2022, **7**, 34966–34973.
2 D. E. Demirocak, S. S. Srinivasan, M. K. Ram, D. Y. Goswami and E. K. Stefanakos, *International Journal of Hydrogen Energy*, 2013, **38**, 1469–1477.
3 B. M. Fung, A. K. Khitrin and K. Ermolaev, *Journal of Magnetic Resonance*, 2000, **142**, 97–101.
4 O. Haidar, T. Roques-Carmes, A. Gouda, N. Tabaja, J. Toufaily and M. Hmadeh, *ACS Applied Nano Materials*, 2024, **7**, 10003–10015.
5 S. Edubilli and S. Gumma, *Separation and Purification Technology*, 2019, **224**, 85–94.
6 A. Huang, L. Wan and J. Caro, *Materials Research Bulletin*, 2018, **98**, 308–313.
7 Y. Cao, H. Zhang, F. Song, T. Huang, J. Ji, Q. Zhong, W. Chu and Q. Xu, *Materials*, 2018, **11**, 589.
8 N. Prasetya and B. P. Ladewig, *Journal of Materials Chemistry A*, 2019, **7**, 15164–15172.
9 V. N. Le, T. K. Vo, K. S. Yoo and J. Kim, *Separation and Purification Technology*, DOI:10.1016/j.seppur.2021.119079.
10 Y. Chang, H. Huang, L. Wang, Y. Li and C. Zhong, *Chemical Engineering Journal*, 2020, **402**, 126201.
11 C. Choi, R. L. Kadam, S. Gaikwad, K.-S. Hwang and S. Han, *Microporous and Mesoporous Materials*, 2020, **296**, 110006.
12 P. Das and S. K. Mandal, *ACS Applied Materials & Interfaces*, 2020, **12**, 37137–37146.
13 C. Gu, Y. Liu, W. Wang, J. Liu and J. Hu, *Frontiers of Chemical Science and Engineering*, 2020, **15**,

437–449.
14 J. M. Park and S. H. Jhung, *Journal of CO2 Utilization*, 2020, **42**, 101332.
15 J. M. Park, D. K. Yoo and S. H. Jhung, *Chemical Engineering Journal*, 2020, **402**, 126254.
16 W.-L. Xue, L. Wang, Y. K. Li, H. Chen, K. X. Fu, F. Zhang, T. He, Y. H. Deng, J. R. Li and C.-Q. Wan, *ACS Sustainable Chemistry & Engineering*, 2020, **8**, 18558–18567.
17 N. Bhoria, J. Pokhrel, S. Anastasiou, K. Suresh Kumar Reddy, G. Romanos and G. N. Karanikolos, *Materials Today: Proceedings*, 2021, **37**, 4044–4048.
18 Z. Gao, L. Liang, X. Zhang, P. Xu and J. Sun, *ACS Appl. Mater. Interfaces*, 2021, **13**, 61334–61345.
19 W.-L. Xue, L. Wang, Y. K. Li, H. Chen, K. X. Fu, F. Zhang, T. He, Y. H. Deng, J. R. Li and C.-Q. Wan, *ACS Sustainable Chem. Eng.*, 2020, **8**, 18558–18567.
20 S. Lamnini, K. Boukayouht, Z. Ouzrour, S. El Hankari, H. Sehaqui and J. Jacquemin, *Langmuir*, 2024, **40**, 14964–14977.